ACS OMEGA

Open Access

http://pubs.acs.org/journal/acsodf

Article

Characterization and Adsorption Capacity of Modified Biochar for Sulfamethylimidine and Methylene Blue in Water

Yao Zheng, Peiyuan Lv, Jie Yang, and Gangchun Xu*

Cite This: *ACS Omega* 2023, 8, 29966−29978

Read Online

ACCESS | Metrics & More | Article Recommendations | Supporting Information

ABSTRACT: In this study, a composite of pond mud and lanthanum- and nano-zero valent iron-modified-biochar was investigated for its ability to adsorb methylene blue (MB) and sulfamethazine (SMZ). La-modified attapulgite and nano-zero valent iron (surface area enhanced by 43.7% via Brunauer−Emmett−Teller analysis) were successfully loaded onto the straw-sediment biochar (BC) surface. With the increase in pyrolysis temperature, the biocompatibility yield, the H, O, and N content, and the ratio of carbon elements decreased, while the pH value, surficial micropores, C element, and ash content increased. The biocarbon small molecules were gradually and tightly ordered, and the organic groups such as hydroxyl, carboxyl groups, and carbon oxygen double bonds were gradually lost or disappeared. The original Fe-BC had more phenolic hydroxyl groups forming an intermolecular hydrogen bond than others with a higher adsorption capacity possibly through the Schiff base reaction. The effect of various pH (2−9), temperature (15−35 °C), and initial concentration (1−25 mg L^{-1}) on adsorption was investigated. pH and temperature were the main factors governing the adsorption process. The maximum adsorption capacity was observed at pH 4. The adsorption performances for MB followed the order Fe-BC > La-BC > BC, and the maximum removal rate was over 98.45% with pH = 7. The three types of BC dosages between 0.2 (6.67 g L^{-1}) and 0.4 g showed a removal rate of 99% for MB. The adsorption capacity of Fe-BC, La-BC, and BC for MB was 2.201, 1.905, and 2.401 mg L^{-1} with pH = 4, while 4.79, 4.58, and 5.55 mg g^{-1} were observed with BC dosage at 0.025 g. For SMZ, the higher the temperature, the better the adsorption effect, and it reaches saturation at approximately 25 °C. To further evaluate the nature of adsorption, Langmuir/Freundlich/Temkin models were tested and the adsorption capacities were evaluated on the surface of the BC composite. The three modified materials were physisorbed to SMZ, while MB was chemisorbed. For MB, the adsorption performance of BC is the best < 0.2 g (6.67 g L^{-1}) at pH 7.0 at 35 °C. The Elovich model was more suitable for MB, while the Freundlich and Temkin models could better fit the adsorption process of MB. The preparatory secondary dynamics equation and Langmuir equation were more compliant for SMZ, and the saturated adsorption capacities of straw-modified, La-BC, and Fe-BC reached 5.699, 6.088, and 5.678 mg L^{-1}, respectively.

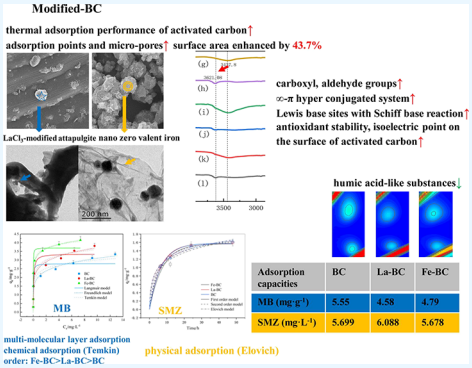

1. INTRODUCTION

Biochar (BC) is a carbon-rich solid product of thermal stabilization of organic matter and is generally used for safe and potentially beneficial storage.[1−3] Activated BC is an efficient adsorbent for removing organic contaminants and other nutrients (N and P) in aquatic environments.[4] Many types of biomass waste, such as agricultural wastes, forestry residues, and sewage sludge can be used to produce BC,[5] and, particularly, surface area affects adsorption efficiency,[6] while wood-based BC increases the C/P ratio and reduces the amount of readily available P,[7] which is attributed to the conversion into bioenergy or to be used as an alternative to chemical fertilizers.[8] In the latter case, conversion should be realized through the implementation of innovative strategies and technologies for the recycling of waste (especially pond mud) as compost and BC for use in aquatic agriculture,[1] which has received increasing attention.[7,9−12]

Ammonium is the most common form of N and contributes to nutrient enrichment in surface waters.[13] However, BC usually has a limited ability to adsorb anions because of its negatively charged surface and poor capacity of anion exchange,[9,14] and metal loading is one type of modification[15] with the reaction between known oxyanions and metal ions or oxides.[16] BCs exhibit a high retention ability owing to high lignocellulose and low ash content,[8] and they present superior abilities (phosphate removal) to remove desirable inorganic ions or organic matter with the addition of functional metal additives (such as CaO, $AlCl_3$, MgO, $MgCl_2$, or Fe_3O_4).[13,17,18] Furthermore, iron modification was done to improve the phosphorus adsorption capacity of BC sludge from lanthanon

Received: February 24, 2023
Accepted: May 3, 2023
Published: August 10, 2023

(La)-involved pyrolysis.[15,19−23] La-BCs allow the loading of lanthanum particles into BC's pore channels and their external surface by supplying many new sites for phosphate adsorption,[15] decreasing the negative charge and repulsive force between phosphate and BC surface, and enhancing the frequency of collisions.[24] The adsorption capabilities of BC vary significantly with the La content and pyrolysis parameters,[15,24,25] and efficient recycling of La-BCs presents significant challenges.[3]

Recent studies on the use of La and magnetic materials with nonbiological materials have addressed the issues of adsorption capacity.[26,27] For example, $La^{3+}/La(OH)_3$ loaded magnetic cationic hydrogel composites,[10] or $La(OH)_3/Fe_3O_4$ nanocomposites[24,28] are used to address these challenges. The adsorption amounts of tetracycline by BC from excess food and garden materials measured by an innovative heat pipe reactor were 2.98 and 8.23 mg g^{-1}, respectively.[29] The maximum adsorption capacities of doxycycline and tetracycline were 128.98 and 104.86 mg g^{-1}, respectively, when BC was loaded with iron with increased surface area and with a large number of carboxyl, hydroxyl and aromatic groups.[2] The use of sulfamethazine (SMZ) affects the pond environment and the quality of fish products.[30−33] More information is needed on the SMZ and sorption capacity of different feedstock materials on SMZ and the effect of pyrolysis temperature on sorption capacity. The amido-functionalized metal−organic framework materials with core/shell magnetic particles had good regeneration and reusability capacity for tetracycline after five cyclic utilization.[34] A previous report found that the rhamnolipid-functionalized graphene oxide hybrid has been demonstrated as a cost-effective and promising sorbent for MB wastewater treatment,[35,36] while Fe_3O_4 modified BC has over 99% of the degradation,[37] and citric acid grafted mobile catalytic materials have the maximum adsorption capacity with a basic pH and temperature of 25 °C.[38] In this study, rice straw and pond sediment were pyrolyzed, then straw BC, La-BC, and nano-zero valent iron (Fe)-modified BC (Fe-BC) were prepared.[3] Their adsorption efficiencies for methylene blue (MB)[35] and SMZ were discussed. The process parameters were optimized by optimizing the experimental conditions, such as the dosage of Fe-BC, initial concentration, and initial pH of the solution. The overall aim of this study was to investigate the effect of BC amendment on SMZ and MB adsorption during composting in laboratory-scale reactors. It has been hypothesized that the addition of BC to composting mixtures prepared from pond mud and rice straw may affect SMZ and MB adsorption during composting.

2. MATERIALS AND METHODS

2.1. BC Preparation and Activation. Feedstock materials, rice straw and mud from tilapia culture ponds, were obtained from FFRC-CAFS in Wuxi, China. The materials were washed with water, air-dried, ground, and sieved to <2.0 mm particles. The sieved materials were placed in ceramic pots in a muffle furnace at different temperatures under a N_2 (purity of 99.99%, 0.1 m^3 h^{-1}) atmosphere to produce BCs. The final pyrolysis temperatures were selected to be 500 °C at a ramping rate of 5 °C min^{-1} and maintained at the highest temperature for 2 h. $LaCl_3{\cdot}7H_2O$ (AR, KeLong Chemical Co. Ltd.) and attapulgite were employed in the pyrolysis for the La-BC preparation. The dried BC (40 g) was immersed in 1000 mL of $LaCl_3$ solution (0.1 M) under magnetic stirring for 6 h. The immersed sawdust afterward was vacuum-filtered and oven-dried at 105 °C for 12 h. Similarly, the BC was also immersed in deionized water (without $LaCl_3$) for comparison with BC preparation. Each of the five BC samples was ground and passed through a 0.5 mm sieve to prepare for the test.

One gram of the as-prepared powder was placed in 50 mL of 1 mol/L each of hydrochloric acid, nitric acid, and phosphoric acid which were then placed in a shaker for 4 h. After suction filtration, the material was washed with distilled water until it was neutral, was placed in an 80 °C oven to dry for 24 h, and placed in a desiccator for later use. To the material, 4 mL of tetra butyl titanate and 2 mL of absolute ethanol were added under vigorous stirring for 30 min to obtain liquid A. Further, 0.4 mL of concentrated nitric acid, 2 mL deionized water, and 17 mL of absolute ethanol were mixed to obtain liquid B. Both the mixtures were mixed under stirring until a transparent sol was obtained. Subsequently, a certain amount of phosphoric acid-activated BC (mass of 0.31, 0.47, 0.94, and 1.88 g, respectively) was added to the sol (the mass fraction of nano-$LaCl_3$ was 75, 67, 50, and 33%, respectively), was fully stirred, dried at 70 °C, and ground to obtain La-BC and Fe-BC (using the same procedure as nano-zero valent iron). $LaCl_3$-modified attapulgite[26,27] and nano zero-valent iron (Beijing Leian Jinbai Technology Co., Ltd), rice straw-pond mud-BC, modified La-BC, and Fe-BC are referred to as groups 1, 2, 3, 4, and 5, respectively.

2.2. BC Characterization. Moisture content was measured by calculating mass loss of the BC upon heating at 105 °C for 24 h to a constant weight. Ash content was also determined by calculating mass loss of the BC upon heating at 750 °C for 5 h. The pH of the BCs was determined in a solution with a mass/water (BC/deionized water) ratio of 1:20 (PHS-3C; LeiCi Instruments Co., Ltd., China). The quantities of the acidic and basic functional groups were measured using the Boehm titration method. After determining the initial pH values of the oxidized BC samples, the BCs were dried at 60 °C for 48 h and then separated into two identical batches. One batch was utilized directly after oxidation and drying (as obtained), while in the other, the pH value was adjusted to 7.00 ± 0.01 using hydrochloric acid (1 M) or sodium hydroxide solution (1 M). The pH values were adjusted every 24 h until they reached equilibrium, and the suspensions were filtered through Whatman No. 1 filter paper and were dried similar to the unadjusted BCs.

Scanning electron microscopy (QUANTA F250 and Hitachi su8010) was performed as previously described.[3] Energy dispersive X-ray spectroscopy (EDS, SU1510, Hitachi, Japan) was performed using the GENESIS energy spectrometer of EDAX company. The specific surface area was determined using N_2 sorption isotherms at 273.15 K (ASAP 2020) and the Brunauer−Emmett−Teller (BET) method using a Quadrasorb Si-MP surface area analyzer. The zeta-potential at pH 7 was determined using a potential analyzer (Zetasizer Nano ZS90), and the values obtained were averaged over three measurements.

The elemental composition (C, H, and N in wt %) of the BCs was determined using an elemental analyzer (EA112, Thermo Finnigan, USA), whereas the O content (wt %) was determined by mass balance, (O = 100 × (C + H + N + ash)).[13] The H/C, O/C, and (O + N)/C atomic ratios were calculated to evaluate the aromaticity and polarity of the BCs. An approximate analysis was performed according to the standard methods in ASTM D 1762-84.

https://doi.org/10.1021/acsomega.3c01251
ACS Omega 2023, 8, 29966−29978

The material surface morphology was analyzed by X-ray powder diffraction (German Bruker D8 Advance),[3] and the chemical compositions were analyzed by X-ray photoelectron spectroscopy (XPS, ESCALAB250Xi, Thermo Fisher Scientific Inc., USA) with Al Kα radiation (1486.6 eV). Fourier transform infrared spectroscopy (FTIR) analysis of the materials was performed using a Vertex70 spectrometer (Thermo Fisher Scientific Co., Ltd.) with KBr as the reference to determine the functional groups of the adsorbents in the wavenumber range of 400−4000 cm^{-1}.[3] Fluorescence excitation emission matrix (EEM)[39] spectroscopy was subsequently conducted using a fluorescence spectrophotometer (Cary Eclipse, Varian Inc., USA) in the scan mode. Interpolation in the affected areas was used to minimize first- and second-order Rayleigh and Raman scattering, and a fluorescence regional integration technique was adopted for analysis.

2.3. MB and SMZ Adsorption. MB ($C_{16}H_{18}ClN_3S{\cdot}3H_2O$) and SMZ ($C_{12}H_{14}N_4O_2S$) were purchased from Tokyo Chemical Industry Co., Ltd. and Shanghai McLean Biochemical Technology Co., Ltd., respectively. The concentration of MB was determined using an ultraviolet spectrophotometer (BioTeke), while for the SMZ, the water sample pretreatment method was followed: 10 mL of water sample was accurately measured in a 50 mL centrifuge tube; 5 mL of methanol and 5 mL of water were used to activate the solid-phase extraction cartridge (Poly-Sery HLB SPE Cartridge 500 mg, 6 mL). The water sample was passed through the column at a flow rate of 2 mL min^{-1}, eluted twice with 5 mL methanol into a 10 mL centrifuge tube (syringe filter 13 mm 0.22 μm) before detection using ultrahigh performance liquid-chromatography/mass spectroscopy (Water UPLC I-Class/XEVO7QD).

In the MB adsorption experiment, the effect of temperature on the adsorption was tested. The shaking time was 24 h, the rotation speed was 200 r min^{-1}, the pH of the initial solution was adjusted to 7 ± 0.2, the initial concentration of MB was 10 mg L^{-1}, and three modified BCs were added with dosage 200 mg. The different temperatures were set at 15, 25, and 35 °C. The effect of the initial MB concentration on the adsorption was tested at a constant temperature of 35 °C, shaking time of 24 h, rotation speed of 200 r min^{-1}, initial solution pH of 7.0 ± 0.2, and the dosages of the three modified BCs were 200 mg. The initial concentrations of MB were 2, 5, 10, 15, 20, 25, 30, and 35 mg L^{-1}. The effect of pH on the adsorption effect was tested at a constant temperature of 25 °C, shaking time of 24 h, rotation speed of 200 r min^{-1}, initial MB concentration of 10 mg L^{-1}, and three modified BC dosages of 200 mg. The pH of the solution was adjusted to 6, 7, 8, and 9 with 0.01 mol L^{-1} HCl and NaOH. The effect of BC dosage on the adsorption effect was tested at a constant temperature of 25 °C, shaking time of 24 h, rotation speed of 200 r min^{-1}, initial solution pH of 7.0, and initial MB concentration of 10 mg L^{-1}. The dosages of the three modified BCs were 0.025, 0.05, 0.1, 0.2, 0.4, and 0.8 g. The solution was filtered through a 0.22 μm water filter, and the MB concentration was measured in the filtrate with a spectrophotometer. Three parallel samples were prepared for all tests, and the test results were averaged.

The predegradation experiment showed 37% (5 d vs 1 d) and 42% (9 d vs 5 d) SMZ (Table S1). An ACQUITY UPLC BEH C18 1.7 μm, 2.1 × 100 mm column was selected as the chromatographic column, and the column temperature was set at 30 °C; the temperature of the autosampler was set to 10 °C, and the injection volume was 5 μL. The gradient elution procedure used solutions A (0.1% formic acid water, 90, 90, 50, 50, 10, 10, 90, and 90%) and B (0.1% formic acid methanol, 10, 10, 50, 50, 90, 90, 10, and 10%), the flow was set at 0.3 mL min^{-1}, and time durations were (initial, 1, 1.01, 3, 3.01, 4.5, 4.51, and 6 min), curve (initial, 6, 1, 6, 1, 6, 6, and 6). Mass spectrometry conditions were: capillary voltage 3.5 kV, taper hole voltage 30 V, ion source temperature 150 °C, desolvent gas temperature 450 °C, desolvent gas flow rate 800 L h^{-1}, and air flow rate in the conical hole 50 L h^{-1}. The parent and daughter ions of SMZ were 254.1458, 155.9746, and 92.0844 m z^{-1}, taper hole voltage was 36 V, collision energies were 28 and 40 V, and the retention time was 0.77 min.

In the adsorption experiment of SMZ, the effect of temperature on the adsorption effect was tested with an oscillation time of 24 h, rotation speed of 220 r min^{-1}, initial solution pH of 4, initial SMZ concentration of 20 mg L^{-1}, and dosages of the three modified BCs were150 mg. Different temperatures at 15, 25, and 35 °C were set in the present study. The effect of the initial concentration of SMZ on the adsorption effect was tested at a constant temperature of 25 ± 1 °C, oscillation time of 24 h, rotation speed of 220 r min^{-1}, default initial solution pH, and the dosages of the three modified BCs were 150 mg. The initial concentrations of SMZ were set to 1, 5, 10, 15, 20, and 25 mg L^{-1}. The effect of pH on the adsorption was tested at a constant temperature of 25 ± 1 °C, oscillation time of 24 h, rotation speed of 220 r min^{-1}, initial SMZ concentration of 20 mg L^{-1}, and the dosages of the three modified BCs were 150 mg. The pH of the solution was adjusted to 2, 4, 7, and 9 with 0.01 mol L^{-1} HCl and NaOH. The effect of BC dosage on the adsorption effect was tested at a constant temperature of 25 ± 1 °C, oscillation time of 24 h, rotation speed of 220 r min^{-1}, initial solution pH of 4, and initial SMZ concentration of 20 mg L^{-1}. We added 0.05 g and 0.07 g of modified carbon.

2.4. Adsorption Kinetics and Dynamic Analysis. A MB standard solution with a concentration of 20 mg L^{-1} was prepared, and the pH of the solution was adjusted to 7 ± 0.2 with 0.01 mol L^{-1} HCl and 0.01 mol L^{-1} NaOH. An amount of 0.2 g of three types of BCs was taken in a 50 mL centrifuge tube to which 30 mL of the as-prepared MB standard solution was added. It was placed in a constant temperature shaker at a rate of 200 r min^{-1} at 35 °C, and reacted for 0.25, 0.5, 1, 1.5, 2, 2.5, 3, 3.5, 4, 4.5, 5, 5.5, and 6 h. The solution was filtered with a 0.22 μm aqueous filter, and the concentration of MB in the filtrate was measured with a spectrophotometer. Three parallel samples were prepared for all tests, and the test results were averaged. The experimental data for MB adsorption were fitted by pseudo-first-order, pseudo-second-order kinetics, and the Elovich equation. To explore the rate-controlling factors in the adsorption process, the data were fitted to an intraparticle diffusion model. MB standard solutions with concentrations of 2, 5, 10, 15, 20, 25, 30, and 35 mg L^{-1} were prepared. The Langmuir, Freundlich, and Temkin adsorption isotherm equations were used to fit and analyze the experimental data for MB adsorption by the three types of BCs.

Based on batch adsorption, the BCs with the highest SMZ adsorption capacity were selected to investigate the adsorption kinetics. The detailed adsorption conditions and initial concentrations of SMZ were identical to those used for batch adsorption. During adsorption, 1 mL samples were periodically withdrawn at 0.25, 0.5, 0.75, 1, 1.5, 2, 3, 4, 8, 12, 24, 36, and 48 h. Two typical models (first-order and second-

https://doi.org/10.1021/acsomega.3c01251
ACS Omega 2023, 8, 29966−29978

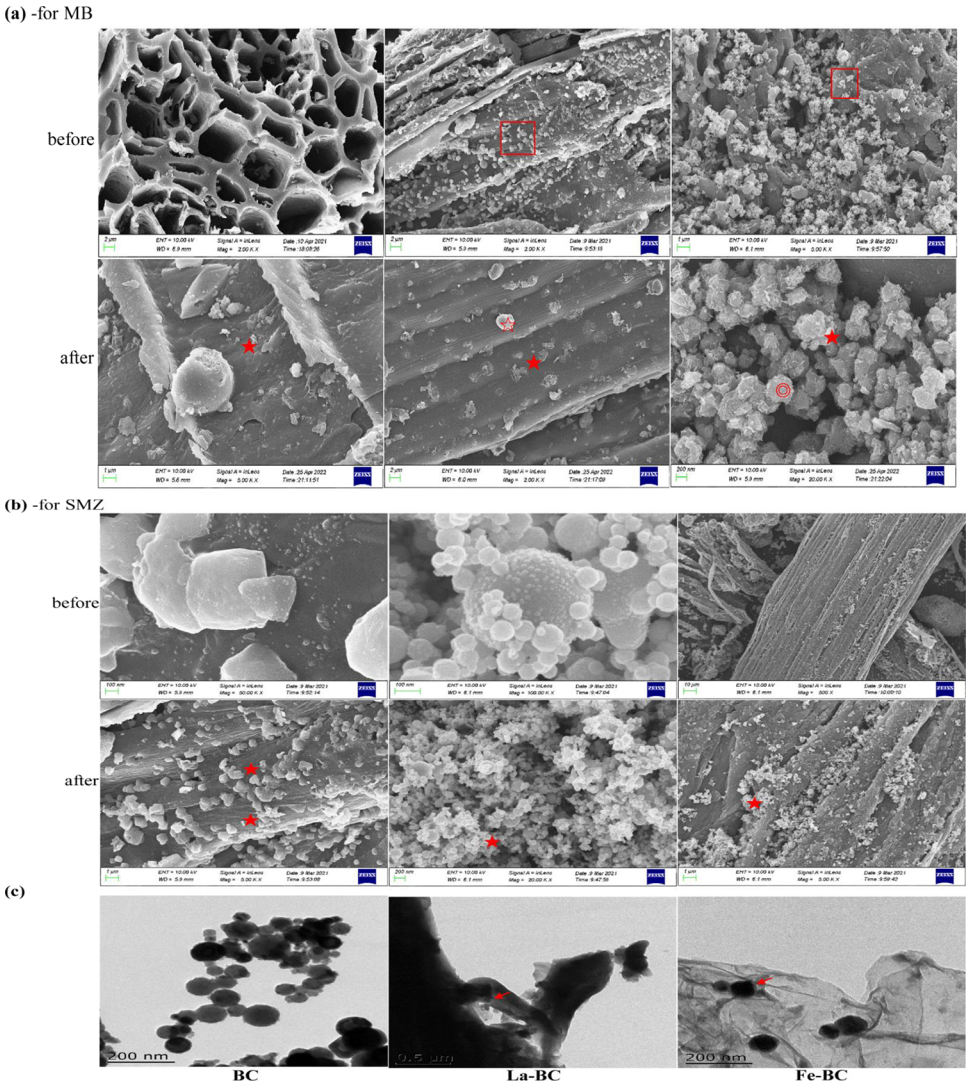

Figure 1. Scanning for MB (a) and SMZ (b) and TEM (c) observation before and after BC modification. a, red star showed the loaded MB, while the red hollow star showed $LaCl_3$-modified attapulgite, and the red double circle showed nano zero valent iron. b, red star showed the loaded SMZ, c, the red arrow revealed the loaded BC in La-BC and Fe-BC.

order) were employed to investigate the adsorption kinetics. SMZ adsorption isotherms were investigated using the selected BCs at 25 ± 0.5 °C. BC (0.1 g) was added to 50 mL of solutions with varying concentrations of SMZ (1−1500 mg L^{-1}). After shaking at 120 rpm for 24 h, samples were withdrawn and filtered to determine their corresponding equilibrium concentrations. Two typical Langmuir and Freundlich isotherm models were used to simulate experimental data. Three-dimensional fluorescence EEM was used to study the aqueous humus-like compounds or aromatic compounds generated during the composting process.[39,40] The location and intensity of fluorescence were analyzed using the methods described in ref 39.

2.5. Data Analysis. The pseudo-first (eq 1) and second-order kinetic 2, Elovich eq 3, and intraparticle diffusion model 4 expressions are:

$$\ln(q_e - q_t) = \ln q_e - k_1 t \tag{1}$$

$$\frac{t}{q_t} = \frac{1}{k_2 q_e^2} + \frac{t}{q_e} \tag{2}$$

$$q_t = \frac{\ln(1 + \alpha\beta t)}{\beta} \tag{3}$$

$$q_t = k_i t^{1/2} + c_i \tag{4}$$

q_e and q_t are the equilibrium adsorption and adsorption amounts (mg g^{-1}). k_1 (min^{-1}) and k_2 (g mg^{-1} min^{-1}) are the pseudo-first- and second-order kinetic model adsorption rate constants, respectively, and α and β are the initial adsorption rates (mg g^{-1} h^{-1}), constants related to the surface coverage (g mg^{-1}). k_i is the intraparticle diffusion rate constant, while c_i is a constant related to the thickness of the adsorption boundary.

The Langmuir (eq 5), Freundlich 6, and Temkin adsorption isotherm 7 equations are:

$$\frac{C_e}{q_e} = \frac{1}{K_L q_{max}} + \frac{C_e}{q_{max}} \tag{5}$$

$$\lg q_e = \lg K_F + \frac{\lg C_e}{n} \tag{6}$$

$$q_e = B(\ln A + \ln C_e) \tag{7}$$

https://doi.org/10.1021/acsomega.3c01251
ACS Omega 2023, 8, 29966−29978

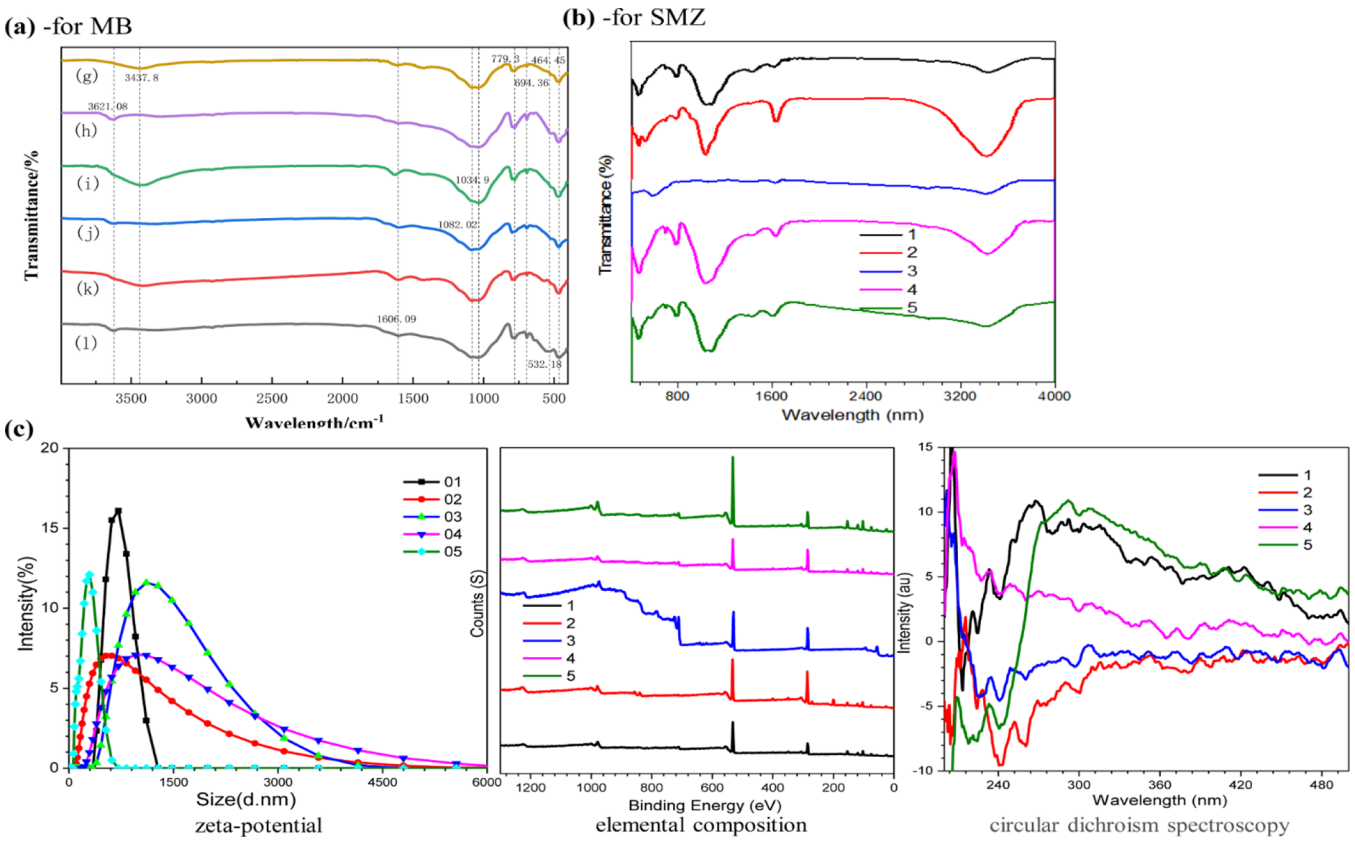

Figure 2. Three kinds of BC characterization. (a) From top to bottom it revealed before and after adsorption in BC, La-BC, and Fe-BC, respectively, via infrared, i.e., g and h showed before and after straw submud BC. (b) FITR spectroscopy, (c) zeta-potential, elemental composition, and circular dichroism spectroscopy for different materials, and the $LaCl_3$-modified attapulgite, nano zero valent iron, rice straw-pond mud-BC, the modified La-BC, and Fe-BC are referred to as group 1, 2, 3, 4, and 5, respectively.

q_{max} is the maximum adsorption capacity (mg g^{-1}), q_e is the equilibrium adsorption capacity (mg g^{-1}), and C_e is the MB equilibrium mass concentration (mg L^{-1}). K_L is the Langmuir equilibrium constant, and K_F is the Freundlich equilibrium constant. n is the Freundlich intensity constant, A is the Temkin equation equilibrium binding constant (L g^{-1}), and B is the Temkin equation coefficient.

Data are presented as mean ± standard error (S.E.). The number of values per group is shown in the table or figure legends. Statistical analysis of the data was performed using one-way analysis of variance. The significance of the results was set at $P < 0.05$.

3. RESULTS

3.1. BC Characterization. It can be seen that BC possesses a large number of irregular pores with a relatively smooth surface (Figure 1a). Spherical substances were attached to the surface of the relatively smooth BC, a chain-like spherical body, indicating that the La-modified attapulgite and nano-zero valent iron were successfully loaded onto the straw-sediment BC surface. The surface of the originally smooth BC appeared crystalline after loading, the voids were reduced, and MB was successfully adsorbed. The surface ratio of BC prepared by mixing rice straw and sediment was uniform (Figure 1b) having voids of different sizes; however, the pore wall was relatively smooth, and there were many surface attachments of small fragments in and near the voids. The number of micropores in the modified BC considerably reduced, and the micropore ratio gradually reduced. The concentration of acidic surface functional groups, especially carboxyl groups of BC increased, and the internal structure of the BC surface also changed, which was convenient for the transformation into medium and large pores from the small micropores of BC. Figure 1b clearly shows that the oxidation treatment led to the destruction of the macropore wall of the original activated carbon. Many pores also began to form slit structures and expanded inward, and the change in surface shape improved the thermal adsorption performance of activated carbon. The BC before and after modification exhibited remarkable difference, and the particle size was approximately 600 μm. The surface was uneven and rough with small holes. Particles with a fibrous rod shape were observed under an electron microscope. The morphology and appearance of the modified BC were considerably different indicating a fine-graining process. Finer particles provided more adsorption points, which could better indicate the adsorption of SMZ.

N_2 adsorption/desorption isotherms were recorded for the BCs (Figure S1). Transmission electron microscopy (TEM) results showed that La-modified attapulgite and nano-zero valent iron were successfully loaded onto the straw-sediment BC surface (Figure 1c). BET results showed 5.72, 0.36, 6.38, 1.47, and 9.17 m^2 g^{-1} for $LaCl_3$-modified attapulgite, nano zero valent iron, rice straw-pond mud-BC, modified La-BC, and Fe-BC, respectively, indicating Fe-BC had higher micropore proportion than the others.

3.2. FTIR and Elemental Analysis. Troughs were observed at approximately 465 (the stretching vibration peak

https://doi.org/10.1021/acsomega.3c01251
ACS Omega 2023, 8, 29966−29978

Table 1. Elemental Analysis

group	C [%]	N [%]	H [%]	O [%]	H/C	O/C	O + N/C
1 ($LaCl_3$-modified attapulgite)	41.81 ± 2.91^a	16.25 ± 0.89^a	4.65 ± 0.28^a	26.62 ± 1.76^a	0.11 ± 0.01^c	0.64 ± 0.07^d	1.03 ± 0.13^d
2 (nano zero valent iron)	13.83 ± 0.78^b	0.19 ± 0.01^c	0.55 ± 0.03^c	19.65 ± 1.06^b	0.04 ± 0.00^d	1.42 ± 0.16^c	1.43 ± 0.12^c
3 (BC)	0.10 ± 0.01^c	0.00^d	2.16 ± 0.14^b	1.32 ± 0.08^d	21.60 ± 0.78^a	13.20 ± 0.69^b	13.20 ± 0.55^b
4 (La-BC)	0.12 ± 0.01^c	0.00^d	0.13 ± 0.01^d	8.24 ± 0.56^c	1.08 ± 0.14^b	68.67 ± 4.32^a	68.67 ± 3.88^a
5 (Fe-BC)	14.45 ± 0.72^b	0.54 ± 0.01^b	0.63 ± 0.01^c	6.79 ± 0.38^c	0.04 ± 0.00^d	0.47 ± 0.11^d	0.51 ± 0.09^d

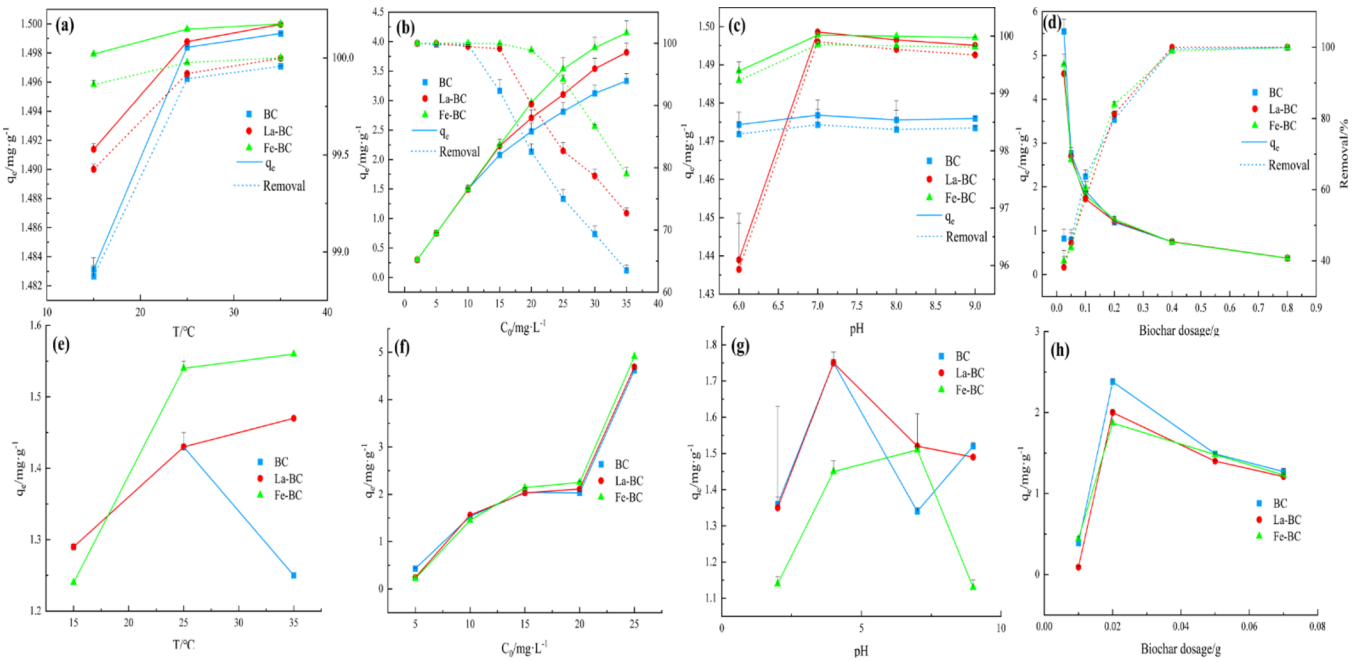

Figure 3. Effects of temperature (a,e), initial concentration (b,f), pH (c,g), and carbon addition (d,h) on the adsorption of MB (a−d) and SMZ (e−h). Rice straw-pond mud-BC, the modified La-BC, and Fe-BC are referred to as group BC, La-BC, and Fe-BC, respectively.

of Si−O−Si), 694 (C−H), 779 (aromatic C−H), 1034 (C−O), 1606 (C═C and C−O), and 3437 (−OH) cm^{-1} for the three BCs (Figure 2a), indicating that the surfaces of the three BCs had the same functional groups, which may be beneficial for sorption. The adsorption result of MB showed that the vibrations around 465, 694, and 779 cm^{-1} were strengthened, and new wave troughs of 3301 and 3621 cm^{-1} appeared around 3437 cm^{-1}; while for La-modified BC, the vibration around 3437 cm^{-1} was weakened, and the trough at 1034 cm^{-1} shifted to 1082 cm^{-1}. New troughs appeared at 3623 and 3332 cm^{-1}, and the trough at 1081 cm^{-1} shifted to the right to 1036 cm^{-1}.

The carboxyl group content in the surface layer decreased significantly compared to other basic functional groups (Figure 2b). The surface layers of carbon materials had groups such as C−O, C═C, C═O, −OH, and C−H, which combined with SMZ through hydrogen bond formation, and the adsorption rate also positively correlated with the amount of functional base. The high-temperature reduction treatment could decompose the carboxyl groups on the surface of the active carbon and the internal aliphatic groups and eliminate the acidic oxygenation functional groups on the adsorption layer of the active carbon, thereby reducing the concentration of these groups. The formation of large lone pair cations and internal groups on the surface of the graphite crucible layer of the active carbon σ electric pair (i.e., ∞-π hyperconjugated system) improved both the Lewis base sites and the antioxidant stability on the surface of activated carbon. Consequently, the isoelectric point of the activated carbon increased.

The characteristic peaks at 3421.60 cm^{-1} (hydroxyl/amino group), 1034.32 cm^{-1} (amide), and 458.75 cm^{-1} (amino), La-BC at 1043 cm^{-1} (aldehyde group) and 1640 cm^{-1} (C═N), 1620 cm^{-1}(C═N and amide regions) and 1656 cm^{-1} (aldehyde) of Fe-BC, and the new peak at 1642 cm^{-1} (C═N, underwent a Schiff base reaction) and 1673 cm^{-1} (aldehyde) were revealed.

The zeta-potential, XPS, and circular dichroism spectroscopy results showed that rice straw-pond mud-BC, modified La-BC, and Fe-BC had good adsorption rates (Figure 2c). With the increase in pyrolysis temperature, the output of primary carbon gradually decreased, the pH value and specific surface area increased, and the C concentration and ash concentration increased (Table 1). The EDS spectrum demonstrated that C and O elements dominated the surface of the BCs, which is in accordance with the results of the elemental analysis. H, the concentration of O, N, and other elements, and the proportion of carbon also decreased with increasing temperature. During pyrolysis, the molecular structure of BC gradually transitioned from disordered to ordered and from a loose alkane structure to a dense aromatic structure. The number of organic groups, such as hydroxyl, carboxyl, and C=O bonds gradually decreased or even disappeared, while the ash concentration gradually increased. At various temperatures, the BC prepared by pyrolysis exhibited a corresponding pH buffer capacity.

https://doi.org/10.1021/acsomega.3c01251
ACS Omega 2023, 8, 29966−29978

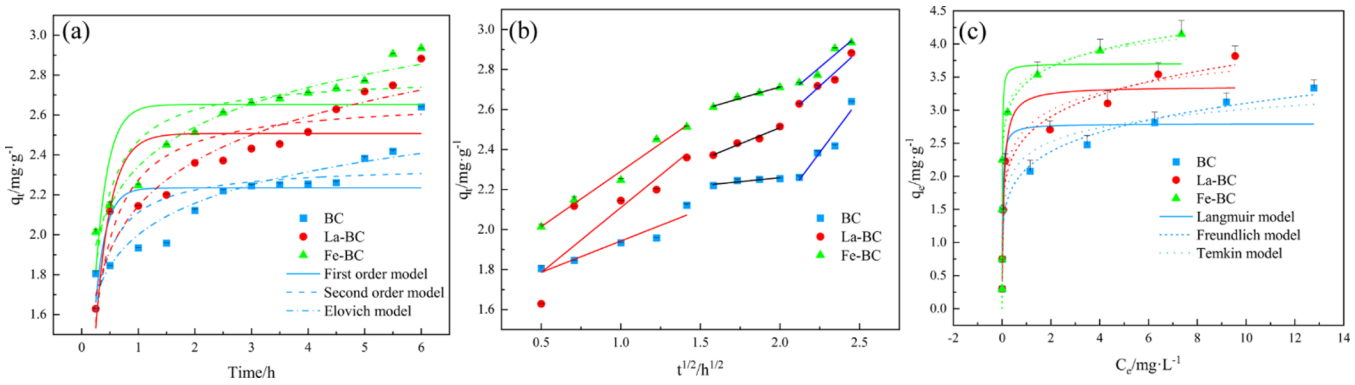

Figure 4. Adsorption kinetics (a), intragranular diffusion (b), and isotherms (c) of three BCs on MB. Rice straw-pond mud-BC, the modified La-BC, and Fe-BC are referred to as group BC, La-BC, and Fe-BC, respectively.

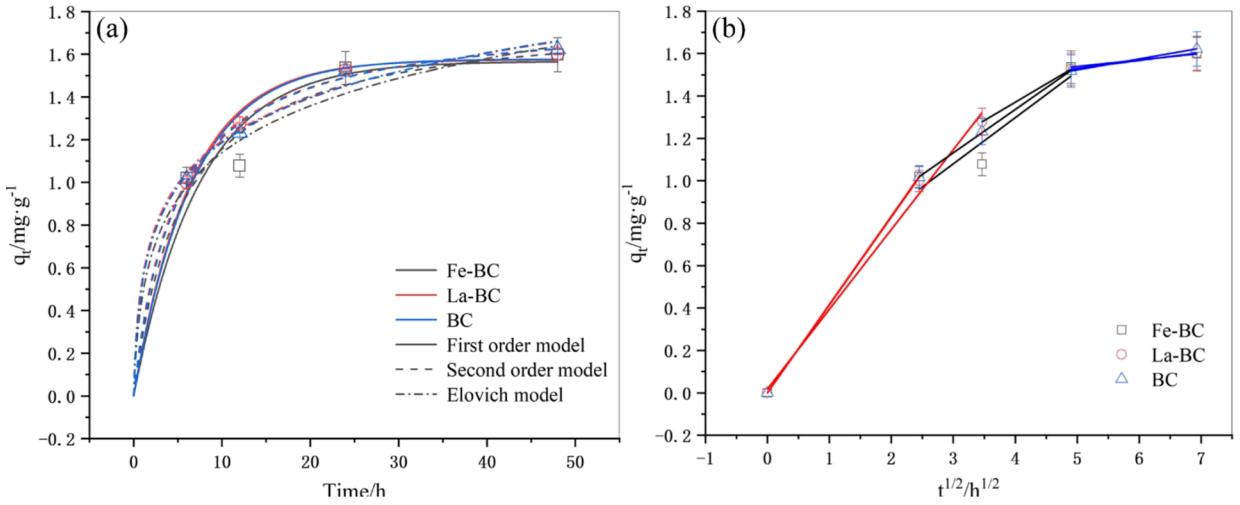

Figure 5. Dynamic model fitting of the modified BCs. (a) Freundlich equation; (b) Langmuir equation; (c) the fitting result of the quasiprimary kinetic model; (d) the fitting of the secondary kinetic model.

3.3. Adsorption Properties of SMZ and MB. The standard curve of SMZ was $y = 2454.2 + 16788x$, and R^2 was 0.96162, while that of MB was $y = 0.2048x + 0.0527$, and R^2 was 0.9963 (Figure S2), indicating that the prepared BCs exhibited good adsorption performance. It can be seen from Figure 3a that with an increase in the adsorption ambient temperature, the removal rate of MB by BC also increased. At 35 °C, the removal rates of MB by the three BCs were higher than those at 15 and 25 °C. When the initial MB concentration was low, the MB removal rate by the three BCs exceeded 99% (Figure 3b), the removal rate of MB by BC decreased with increasing MB concentration. Thus, the adsorption capacity (the equilibrium adsorption capacity 0.3 to 3.33 mg g^{-1}) continued to increase. The removal rate of sediment BC was approximately 100% and decreased to 92.35% when the MB concentration was less than or equal to 10 mg L^{-1}, and finally reached 15 mg L^{-1}. For La-BC and Fe-BC, when the MB concentration was less than or equal to 15 or 20 mg L^{-1}, the removal rate of MB for both was ∼100%, and these declines were 90.18% (0.3 to 3.81 mg g^{-1}) and 98.88%, respectively. The equilibrium adsorption capacity of MB on carbon increased from 0.3 to 4.14 mg g^{-1} (25 mg L^{-1}). The equilibrium adsorption capacity of modified BC was always higher than that of original BC, indicating that modification could indeed improve the adsorption performance of BC. Overall, the adsorption performances of the three samples followed the order Fe-BC > La-BC > BC. When the initial pH of the MB solution increased from 6 to 9, the removal rate was as high as 98% (98.45, 99.90, and 99.85% for BC, La-BC, and Fe-BC at pH = 7, Figure 3c). In the experiment using 30 mL of 10 mg L^{-1} MB solution, the removal rate of MB by BC (5.55, 4.58, and 4.79 mg g^{-1} to 1.19, 1.21, 1.25 mg g^{-1}) increased with increasing dosage (from 0.025 to 0.2 g), and the adsorption performance of modified BC was better than that of unmodified BC (Figure 3d). When the dosages of BC were 0.2 and 0.4 g, the MB removal rates by the three types of BC were 79.63, 81.19, and 83.90% and 99.42, 100, and 98.90%, respectively. When the dosage of BC reaches 0.8 g, it reached a state of supersaturation, so the increase was significantly lower than that of 0.025−0.4 g dosage. Considering the comprehensive benefits such as rationality and economy, it is considered appropriate to use 0.2 g (6.67 g L^{-1}) BC in the experiment.

The higher the temperature, the better the adsorption effect, which reached saturation at approximately 25 °C (Figure 3e). The activity of oxygen-containing functional groups on the surface reduced the adsorption effect to a certain extent at 25 °C. The high temperature enhanced the binding effect between the surface functional groups of the modified BC and ions in the SMZ. When the temperature reached 35 °C, the adsorption by the three modified BCs was close to saturation and there was no obvious effect. When the initial concentration

https://doi.org/10.1021/acsomega.3c01251
ACS Omega 2023, 8, 29966−29978

Table 2. Fitting Parameters of Adsorption Kinetics for MB by Three BCs Obtained from the Langmuir, Freundlich, and Temkin Isotherm Models

					first stage			Langmuir model		
isotherm model	sample	k_1/min^{-1}	q_e/mg g^{-1}	R^2	k_1/mg g^{-1} h^{-1}	c_1	R^2	q_{max}/mg g^{-1}	K_L/L mg^{-1}	R^2
first-order model	BC	5.43	2.23	0.32	0.31	1.63	0.90	2.79	41.61	0.81
	La	3.77	2.51	0.62	0.65	1.46	0.77	3.36	14.57	0.83
	Fe	4.59	2.65	0.51	0.55	1.74	0.98	3.70	105.79	0.74
					second stage			Freundlich model		
		K_2/g mg^{-1} min^{-1}	q_e/mg g^{-1}	R^2	k_2/mg g^{-1} h^{-1}	c_2	R^2	K_F	$1/n$	R^2
second-order model	J	3.74	2.35	0.62	0.08	2.10	0.85	2.12	0.17	0.96
	La	2.08	2.68	0.81	0.32	1.86	0.97	2.61	0.15	0.93
	Fe	2.67	2.80	0.80	0.23	2.25	0.98	3.42	0.10	0.81
					third stage			Temkin model		
		α/mg g^{-1} h^{-1}	β/g mg^{-1}	R^2	k_3/mg g^{-1} h^{-1}	c_3	R^2	A/L g^{-1}	B	R^2
Elovich model	J	1468.32	4.39	0.85	1.07	−0.02	0.91	1938.20	0.31	0.95
	La	236.36	3.07	0.92	0.72	1.09	0.94	7293.21	0.38	0.92
	Fe	1020.55	3.49	0.97	0.67	1.30	0.93	1.22×10^5	0.30	0.80

Table 3. Sorption Parameters of SMZ by Three BCs Obtained from the Langmuir and Freundlich Isotherm Models[a]

isotherm model	sample	Q	$K_1/2$	R1/2	Qm/n	K	Ra/b
first-order model	J	0.07885	0.15133	0.98739	11.61060	0.00433	0.99993
	La	0.07870	0.15579	0.99546	12.90450	0.00390	0.99995
	Fe	0.07834	0.13543	0.95403	19.38620	0.00259	0.99998
second-order model	J	0.08945	2.32421	0.99734	1.00000	0.05000	1.00000
	La	0.08900	2.43148	0.99868	1.00000	0.05000	1.00000
	Fe	0.08930	2.05763	0.97062	1.00000	0.05000	1.00000

[a]Note: R1 and R2 stand for the correlation coefficient of the Langmuir isotherm model, and *Ra* and *Rb* stand for the correlation coefficient of the Freundlich isotherm model.

was 10 mg L^{-1}, the adsorption rate was higher (Figure 3f). The effect of pH on the adsorption effect showed that with an increase in pH, the adsorption capacity of Fe-BC decreased from 2.201 to 1.232 mg L^{-1}, that of La modification decreased from 1.905 to 1.327 mg L^{-1}, and that of straw modification decreased from 2.401 to 1.454 mg L^{-1}, because the low crosslinking density consumed the least number of antibiotic active sites on the modified BC chain. The modified BC had a certain adsorption effect between pH = 4−10, and the adsorption performance of the modified BC also had a certain pH stability. At pH 4, the antibiotic solution exhibited the best adsorption performance (Figure 3g) for both straw-modified BC and La-BC, but Fe-BC performs well between pH 4 and 7. When the dosage of the drug was 10 mg L^{-1}, the BC dosage of 0.02 g was best (Figure 3h). Straw-modified BC had a better adsorption of adsorbent materials exhibiting good balance between strength and toughness.

3.4. Adsorption Kinetics of SMZ and MB in BC. The Langmuir (R^2 = 0.81, 0.83, 0.74), Freundlich (R^2 = 0.96, 0.93, 0.81), and Temkin (R^2 = 0.95, 0.92, 0.80) models were more in line with the three BCs (Figure 4). The adsorption of MB by the three BCs belonged to multimolecular layer adsorption that occurred on the inhomogeneous surface. The higher values for Fe/La-BC in the Temkin model indicate that the experimental adsorption process belongs to chemical adsorption with a strong electrostatic effect, and the adsorption performance of the modified BCs in the test is much better than that of the unmodified BC.

In the initial stage, the antibiotic adsorption capacity increased rapidly with time as the initial concentration of antibiotics was high (Figure 5). After 24 h, equilibrium was reached, and the maximum adsorption capacity was slowly reached. This slow process was due to the decrease in solution concentration and the large number of adsorption sites on the surface of the modified BC, lowering the adsorption capacity of the whole adsorbent for antibiotics. Moreover, antibiotics need to penetrate deeper into the modified BCs to reach the adsorption sites and stabilize them. Once all the adsorption sites of the modified BCs were occupied, adsorption equilibrium was reached. After the concentration calculation, the saturated adsorption capacities of straw-modified BC, La-BC, and Fe-BC reached 5.699, 6.088, and 5.678 mg L^{-1}, respectively.

Compared with the quasi-first-order kinetic equation, the adsorption capacity calculated by the quasi-second-order kinetic equation was closer to the experimental observation value (Table 2). The correlation coefficient between the quasi-second-order adsorption and kinetic models was higher than that of the standard-level kinetic model. The R^2 of the Elovich model was higher, indicating that the adsorption behavior of the Elovich model on the MB adsorption by the three BCs is comparable to that of the first-order and pseudo-second-order kinetic models (Table 3). These observations indicated that the adsorption of MB is nonuniform chemical adsorption. The correlation coefficients fitted by the Langmuir adsorption isotherm model were 0.99998 for straw-modified BC, 0.99995 for La-BC, and 0.99993 for Fe-BC. The R^2 of the quasi-second-order kinetic model was 0.99734 for straw modification, 0.99868 for La-BC, and 0.97062 for Fe-BC.

The linear intercepts of the three types of BC fitting intraparticle diffusion equations are not zero, indicating that "intragranular diffusion" is not the only controlling step, and

https://doi.org/10.1021/acsomega.3c01251
ACS Omega 2023, 8, 29966−29978

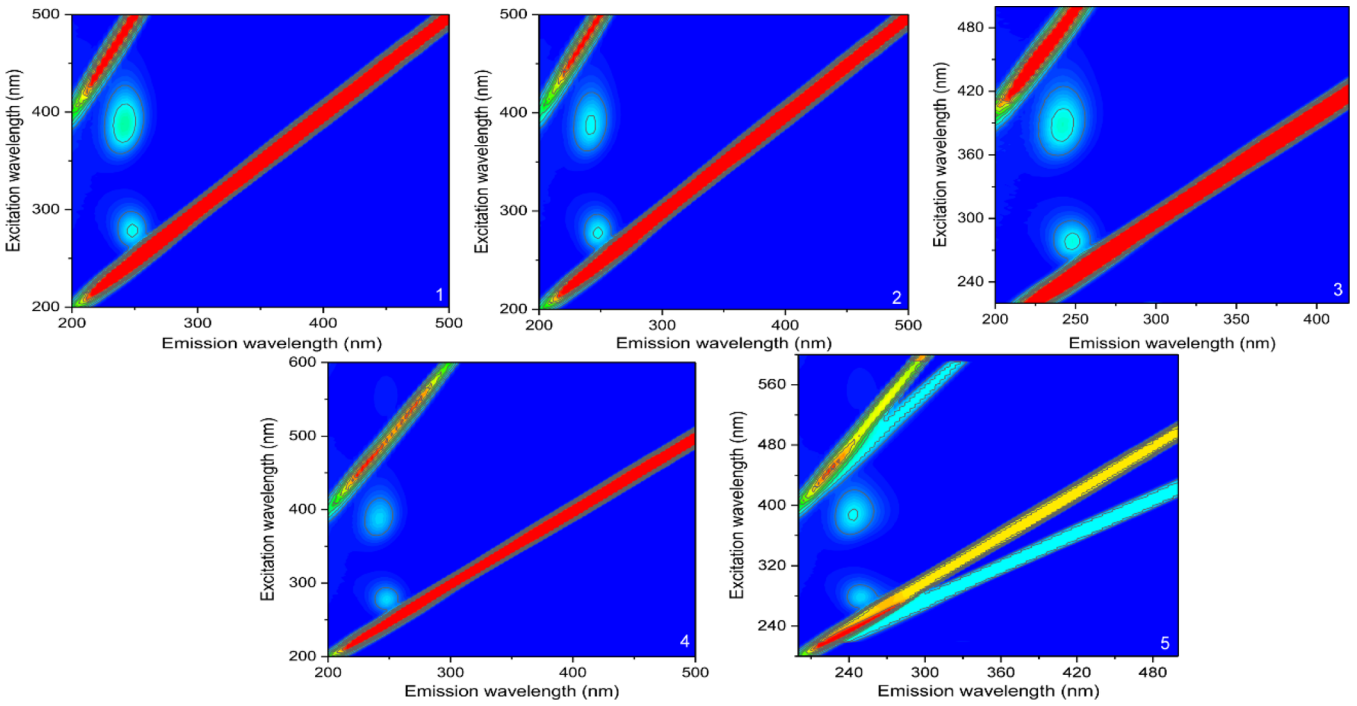

Figure 6. EEM spectra of primary BC and modified BCs. $LaCl_3$-modified attapulgite, nano zero valent iron, rice straw-pond mud-BC, the modified La-BC, and Fe-BC are referred to as group 1, 2, 3, 4, and 5, respectively.

thin-film diffusion is also involved. The fitting parameter table of the intraparticle diffusion model for MB adsorption by BC shows that the k_i value of the third stage was larger than that of the first two stages, indicating that the adsorption rate of the third stage was higher than those of the first and second stages. The fluorescence intensity of those regions had declined (Figure 6).[39,40] The easily degradable organic matter components such as humic acid-like substances decreased.[40] These results suggest that the transformation of fluorescence from the fulvic-acid-like region to the humic-acid-like region was continuous and flowing.[40]

4. DISCUSSION

4.1. Modified BC Characteristics Facilitated Adsorption. The density of the porous structure was higher for Fe-BC than La-BC, and that of straw-modified BC was the smallest. These modified BCs had larger specific surface areas, with more exposed active sites becoming denser due to the development of a three-dimensional network structure.[41] The layered structure disappeared and a denser porous structure was produced with an increase in the amount of La-BC and Fe-BC, but the disappearance of the layered structure in Fe-BC occurred slightly later than that of La-BC. The original Fe-BC had more phenolic hydroxyl groups forming an intermolecular hydrogen bond than La-BC, but the crosslinking (relative to amino groups) density was lower. FTIR spectra showed that the modified BC chain was grafted onto the modified BC chain through a Schiff base reaction[42] and the modified BC chain was developed into a three-dimensional network through hydrogen bonding.

The elemental change results showed that with an increase in pyrolysis temperature,[43] the biocompatibility yield decreased, while the pH value and surface area increased, and the concentration of C and ash also increased. With an increase in temperature, the H/C, O/C, and O + N/C ratios decreased in the Fe-BC group.[44,45] During pyrolysis, the structure changed from a loose alkane to a dense aromatic structure. The organic groups such as hydroxyl, carboxyl, and C═O bonds gradually decreased and even disappeared, indicating that the synthesized modified BCs had solid photolysis characteristics to ensure the stability of the modified BCs in the adsorption process. La-BC had a lower crosslinking density than the other two groups of modified BC, which may lead to excessive photolysis in the antibiotic adsorption stage, which was not conducive to the adsorption by the modified BC. It can be concluded that cation exchange, complexation with surface functional groups, and precipitation with minerals were the dominant mechanisms responsible for MB and SMZ adsorption by straw and pond mud-BC (Figure 7).[45]

4.2. pH Affecting BC's Adsorption Efficiency. Temperature, modified BC dosage, and SMZ concentration reflected the active amount of elements involved in the adsorption process.[46] The results not only showed the best value of the prepared modified BCs as an adsorbent, but also reflected the environmental condition and dosage suitable for the adsorption by the modified BC. The pH value also directly affects the surface charge of the absorbent and the retention of antibiotics in water.[47] The effect is better under acidic environment particularly at pH = 4, because the acidic environment is conducive to the protonation of amino groups on the modified BC, and the protonated amino groups provide a driving force for the antibiotic adsorption process. However, the acidic environment is not conducive to the stability of the Schiff base bond, but to the transformation of the acid-soluble fraction to oxidizable and residual fractions.[2] The adsorption effect of Fe-BC was weaker than that of La-BC (similar to the straw-modified BC), which was different from the study performed using Fe_3O_4 modified BC.[37] A previous study found a mobile catalytic material has the maximum adsorption at a basic pH,[38] and then, with the increase in pH in the present

https://doi.org/10.1021/acsomega.3c01251
ACS Omega 2023, 8, 29966−29978

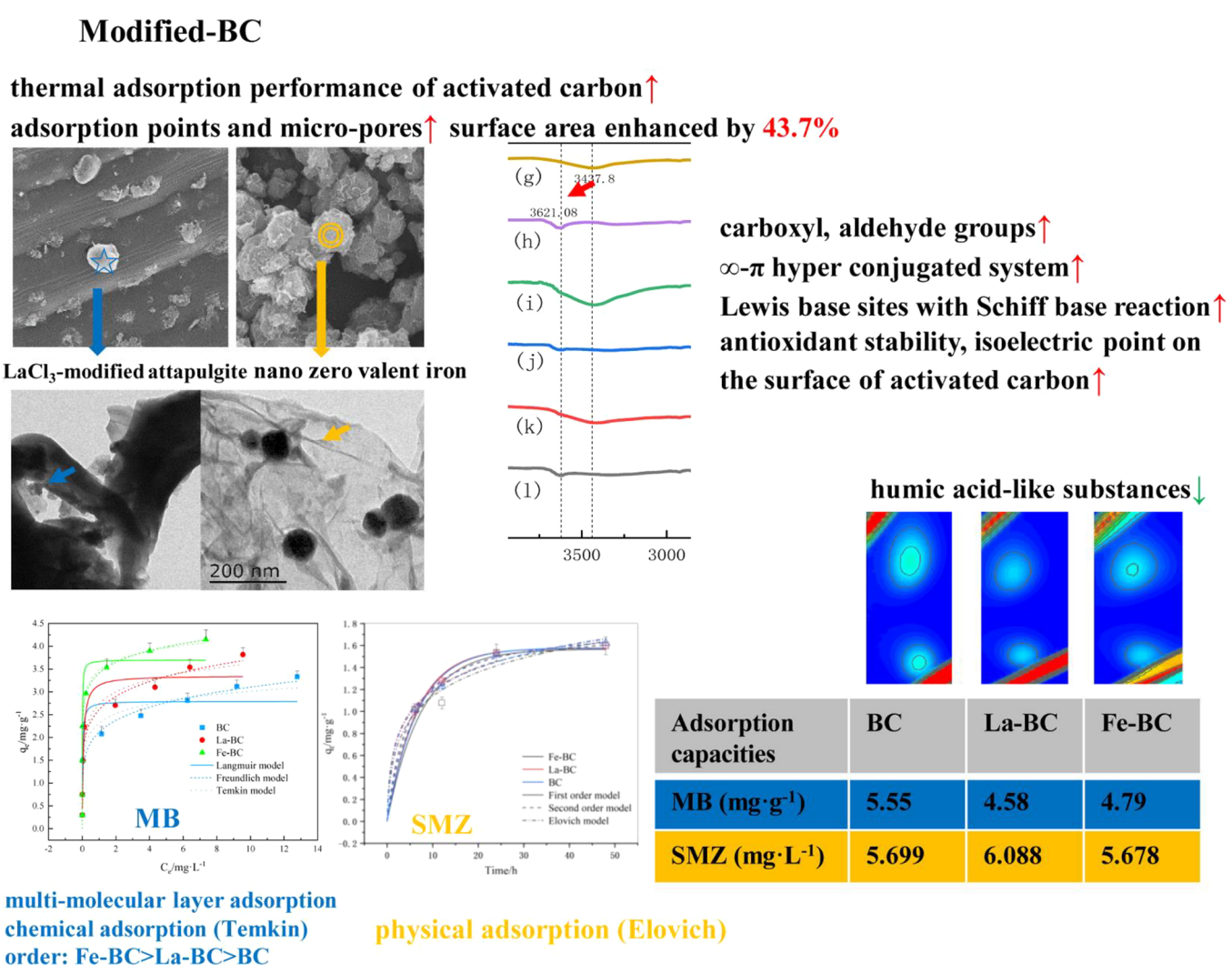

Adsorption capacities	BC	La-BC	Fe-BC
MB (mg·g^{-1})	5.55	4.58	4.79
SMZ (mg·L^{-1})	5.699	6.088	5.678

Figure 7. Possible mechanisms of sulfamethylimidine and MB degradation by BC catalysts.

study, the antibiotic adsorption capacity per unit mass of the modified BCs decreased because the amino group lost its electrostatic attraction to antibiotics due to deprotonation.

4.3. Kinetics Model and Adsorption Process. The study of adsorption kinetics showed that the adsorption effect of modified BC on SMZ was related to the residence time of antibiotics at the solid−liquid interface. The process of removing antibiotics from sewage by absorbing substances can be expressed by a quasi-first-order or quasi-second-order adsorption kinetic equation, which is termed as physical adsorption. Van der Waals forces are mainly used as the driving forces for antibiotic adsorption.[48] The quasi-second-order adsorption kinetic model suggests that antibiotic adsorption is dominated by chemical forces, and the entire process is irreversible without changing environmental conditions.[12,49] The biological adsorption process is more suitable for the quasi-second-order adsorption kinetic process, whereas the biochemical adsorption process dominates the entire adsorption process, and electrostatic attraction is the main driving force of antibiotic adsorption. Regarding the mode of action, some reports have shown that electrostatic interactions, H-bonding, and $\pi-\pi$ interactions are the main interactions between SMZ and BC.[50] $-NH_2$, $-OH$, and some oxygen-containing groups,[51] electron donor−acceptor interactions and hydrogen bonds,[52] electrostatic interactions, ligand exchange or complexation,[25] metolachlor, hydrogen bonds, $\pi-\pi$ bonds, coordination bonds, and hydrophobic interactions[53] are also responsible for the enhanced chemical adsorption based removal[51] with aromatic functional groups.[54,55] The adsorption process completely satisfied the Langmuir adsorption isotherm model and quasi-second-order adsorption kinetics, which showed that the adsorption process of modified BC for SMZ was monolayer adsorption dominated by chemical adsorption and electrostatic attraction. The existing more intermolecular hydrogen bond may activate the reaction between the amino group and the aldehyde group, shape with a dense ordered aromatic structure, and evoke a Schiff base reaction. This process is accomplished by enhancing chemical adsorption, instead of the effects from coexisting anions and organics.

The three groups of modified BCs had good antibiotic removal abilities. However, to improve the yield and adsorption characteristics of bioactive carbon by screening adsorbents and modification methods, the adsorption principle (the decreased humic-acid-like region via EEM)[39,40] and the site of BC modification need to be further studied. Lots of reports demonstrated metal−organic framework materials[34] and rhamnolipid-functionalized graphene oxide hybrid[36] had good regeneration and reusability capacity. The regeneration and utilization of modified activated carbon are key factors in considering the economic performance of the adsorption

https://doi.org/10.1021/acsomega.3c01251
ACS Omega 2023, 8, 29966−29978

process. Our recent study showed Al-impregnated thermally treated calcium-rich attapulgite (Al@TCAP-N) and volcanic stone had good regeneration performance,[56] which was used for wastewater treatment.[57−66] Therefore, when we used it in the sedimentation unit, its recycling and regeneration ability is worth discussing based on the excellent adsorption capacities when compared with other reports (MB[36,59−63] and sulfamethylimidine,[55,64−66] Table 4). However, with regard to desorption and recycling, iron modification and La modification cannot be reused. This is because the strong hydrogen bonds in the iron modification make the modified BC very rigid when constructing the network, which greatly reduces its ductility. The strong crosslinking density in La modification causes the modified BC to maintain its inherent strength during the reaction, making it unable to react again during the adsorption process. The modified BC must have a good balance between strength and toughness to ensure its integrity and adsorption efficiency for multiple cycles. Based on this study, it is also suggested to further investigate the effect of coexisting anions and organics for the MB and SMZ treatments, and the use of modified BC in real antibiotics, printing, and dyeing wastewater.

Table 4. Comparison of the Obtained Results with Other Adsorption Capacities

comparison	MB in this study	SMZ in this study
this study	6.67 g L^{-1}	6.09 mg L^{-1}
Wu et al.[36]	0.32 g L^{-1}	
Jiang et al.[59]	197.4 g L^{-1}	
Hoslett et al.[60]	7.20 g L^{-1}	
Zhang et al.[61]	862 g L^{-1}	
Xi et al.[62]	300.36 g L^{-1}	
Diaz-Uribe et al.[63]	2.94 g L^{-1}	
Rajapaksha et al.[55]		37.70 mg L^{-1}
Deng et al.[64]		7.004 mg L^{-1} (sulfamethazine)
Tian et al.[65]		9.84 mg L^{-1} (sulfamethoxazole)
Lin et al.[66]		21.70 g L^{-1} (sulfamethoxazole)

5. CONCLUSIONS

With an increase in the thermal decomposition temperature, the biological properties of the product decreased, and the pH value, specific surface area, and the C and ash contents increased. The slowly decomposing small molecules of BC gradually change from a disordered state to an ordered state, and the alkane structure gradually changes to an organic aromatic structure in the form of high-density hydroxyl/carboxyl groups and C═O double bonds. Crystallized substances, adsorption sites appeared on the surface of the originally smooth BC following adsorption and the voids were reduced. In the adsorption experiment of SMZ by BC, the higher the temperature, the better the adsorption effect, and it reached saturation at approximately 25 °C at pH = 4, with BC addition amount = 0.02 g (10 mg L^{-1}). The adsorption performance of MB by BC is the best when the addition amount is 0.2 g (6.67 g L^{-1}), pH =7.0, temperature = 35 °C. The three modified BCs play a leading role in the physical adsorption of SMZ and the chemical adsorption of MB. The pseudo-second-order kinetic equation is more conducive to explain the entire adsorption process of SMZ, and the Langmuir equation is more in line with the adsorption of SMZ by the modified BC. On the other hand, the Elovich model is better than the pseudo-first-order and pseudo-second-order models to fit the adsorption behavior of MB by BCs, and the Freundlich and Temkin models are more suitable for explaining the adsorption of MB.

■ ASSOCIATED CONTENT

Supporting Information

The Supporting Information is available free of charge at https://pubs.acs.org/doi/10.1021/acsomega.3c01251.

Figure S1: N2 adsorption/desorption isotherm. The $LaCl_3$-modified attapulgite, nano zero valent iron, rice straw-pond mud-BC, the modified La-BC, Fe-BC are referred to as group 1, 2, 3, 4 and 5, respectively; Figure S2: The standard curves for MB and SMZ; Table S1" Pre-experiment for degradation of the sulfoma (PDF)

■ AUTHOR INFORMATION

Corresponding Author

Gangchun Xu − *Key Laboratory of Integrated Rice-Fish Farming Ecology, Ministry of Agriculture and Rural Affairs, Freshwater Fisheries Research Center (FFRC), Chinese Academy of Fishery Sciences (CAFS), Wuxi, Jiangsu 214081, China; Wuxi Fishery College, Nanjing Agricultural University, Wuxi, Jiangsu 214081, China;* orcid.org/0000-0003-1861-3692; Phone: +86-510-85551464; Email: xugangchun1979@163.com; Fax: +86-510-85551424

Authors

Yao Zheng − *Key Laboratory of Integrated Rice-Fish Farming Ecology, Ministry of Agriculture and Rural Affairs, Freshwater Fisheries Research Center (FFRC), Chinese Academy of Fishery Sciences (CAFS), Wuxi, Jiangsu 214081, China; Wuxi Fishery College, Nanjing Agricultural University, Wuxi, Jiangsu 214081, China;* orcid.org/0000-0001-5958-6008

Peiyuan Lv − *Wuxi Fishery College, Nanjing Agricultural University, Wuxi, Jiangsu 214081, China*

Jie Yang − *Wuxi Fishery College, Nanjing Agricultural University, Wuxi, Jiangsu 214081, China*

Complete contact information is available at: https://pubs.acs.org/10.1021/acsomega.3c01251

Author Contributions

Y.Z. and G.C.X. conceived and designed the experiments; Y.Z. analyzed the data; P.Y.L. and J.Y. contributed reagents/materials/analysis tools; Y.Z. contributed to the preparation of tables; and Y.Z. prepared and wrote the manuscript. All authors have reviewed the manuscript.

Notes

The authors declare no competing financial interest.

■ ACKNOWLEDGMENTS

The work was supported by the China Agriculture Research System of MOF and MARA (No. CARS-46), Central Public-interest Scientific Institution Basal Research Fund, Freshwater Fisheries Research Center, CAFS (NO. 2021JBFM19), and the open project of Agriculture Ministry Key Laboratory of Healthy Freshwater Aquaculture (ZJK202102). We thank Sampriti (english editors both working for Editage) for providing grammar and spelling check of the manuscript.

https://doi.org/10.1021/acsomega.3c01251
ACS Omega 2023, 8, 29966−29978

REFERENCES

(1) Bolan, N.; Hoang, S. A.; Beiyuan, J.; Gupta, S.; Hou, D.; Karakoti, A.; Joseph, S.; Jung, S.; Kim, K.; Kirkham, M.; Kua, H. W.; Kumar, M.; Kwon, E. E.; Ok, Y. S.; Perera, V.; Rinklebe, J.; Shaheen, S. M.; Sarkar, B.; Sarmah, A. K.; Singh, B. P.; Singh, G.; Tsang, D. C. W.; Vikrant, K.; Vithanage, M.; Vinu, A.; Wang, H.; Wijesekara, H.; Yan, Y.; Younis, S. A.; Van Zwieten, L. Multifunctional applications of biochar beyond carbon storage. *Int. Mater. Rev.* **2022**, *67*, 150−200.

(2) Gopinath, A.; Divyapriya, G.; Srivastava, V.; Laiju, A. R.; Nidheesh, P. V.; Kumar, M. S. Conversion of sewage sludge into biochar: A potential resource in water and wastewater treatment. *Environ. Res.* **2021**, *194*, No. 110656.

(3) Li, C.; Huang, Q.; Zhang, H.; Wang, Q.; Xue, R.; Guo, G.; Hu, J.; Li, T.; Wang, J.; Hu, S. Characterization of biochars produced by co-pyrolysis of hami melon (cantaloupes) straw mixed with polypropylene and their adsorption properties of cadmium. *Int. J. Environ. Res. Public Health* **2021**, *18*, 11413.

(4) Tan, X.; Liu, Y.; Zeng, G.; Wang, X.; Hu, X.; Gu, Y.; Yang, Z. Application of biochar for the removal of pollutants from aqueous solutions. *Chemosphere* **2015**, *125*, 70−85.

(5) Xiao, R.; Awasthi, M. K.; Li, R.; Park, J.; Pensky, S. M.; Wang, Q.; Wang, J. J.; Zhang, Z. Recent developments in biochar utilization as an additive in organic solid waste composting: A review. *Bioresour. Technol.* **2017**, *246*, 203−213.

(6) Dou, S.; Ke, X. X.; Shao, Z. D.; Zhong, L. B.; Zhao, Q. B.; Zheng, Y. M. Fish scale-based biochar with defined pore size and ultrahigh specific surface area for highly efficient adsorption of ciprofloxacin. *Chemosphere* **2022**, *287*, No. 131962.

(7) Chen, Z.; Jin, P.; Wang, H.; Hu, T.; Lin, X.; Xie, Z. Ecoenzymatic stoichiometry reveals stronger microbial carbon and nitrogen limitation in biochar amendment soils: A meta-analysis. *Sci. Total Environ.* **2022**, *838*, No. 156532.

(8) Babu, S.; Singh Rathore, S.; Singh, R.; Kumar, S.; Singh, V. K.; Yadav, S. K.; Yadav, V.; Raj, R.; Yadav, D.; Shekhawat, K.; Ali Wani, O. Exploring agricultural waste biomass for energy, food and feed production and pollution mitigation: A review. *Bioresour. Technol.* **2022**, *360*, No. 127566.

(9) Cui, X.; Hao, H.; Zhang, C.; He, Z.; Yang, X. Capacity and mechanisms of ammonium and cadmium sorption on different wetland-plant derived biochars. *Sci. Total Environ.* **2016**, *539*, 566−575.

(10) Dong, S.; Wang, Y.; Zhao, Y.; Zhou, X.; Zheng, H. La^{3+}/$La(OH)_3$ loaded magnetic cationic hydrogel composites for phosphate removal: effect of lanthanum species and mechanistic study. *Water Res.* **2017**, *126*, 433−441.

(11) Fang, L.; Wu, B.; Chan, J. K. M.; Lo, I. M. C. Lanthanum oxide nanorods for enhanced phosphate removal from sewage: a response surface methodology study. *Chemosphere* **2018**, *192*, 209−216.

(12) Hamadeen, H. M.; Elkhatib, E. A. New nanostructured activated biochar for effective removal of antibiotic ciprofloxacin from wastewater: Adsorption dynamics and mechanisms. *Environ. Res.* **2022**, *210*, No. 112929.

(13) Li, R.; Wang, J. J.; Zhou, B.; Awasthi, M. K.; Ali, A.; Zhang, Z.; Gaston, L. A.; Lahori, A. H.; Mahar, A. Enhancing phosphate adsorption by Mg/Al layered double hydroxide functionalized biochar with different Mg/Al ratios. *Sci. Total Environ.* **2016**, *559*, 121−129.

(14) Xu, D.; Cao, J.; Li, Y.; Howard, A.; Yu, K. Effect of pyrolysis temperature on characteristics of biochars derived from different feedstocks: A case study on ammonium adsorption capacity. *Waste Manage.* **2019**, *87*, 652−660.

(15) Liao, T.; Li, T.; Su, X.; Yu, X.; Song, H.; Zhu, Y.; Zhang, Y. $LaOH_3$-modified magnetic pineapple biochar as novel adsorbents for efficient phosphate removal. *Bioresour. Technol.* **2018**, *263*, 207−213.

(16) Cho, D. W.; Yoon, K.; Ahn, Y.; Sun, Y.; Tsang, D. C. W.; Hou, D.; Ok, Y. S.; Song, H. Fabrication and environmental applications of multifunctional mixed metal-biochar composites (MMBC) from red mud and lignin wastes. *J. Hazard. Mater.* **2019**, *374*, 412−419.

(17) Dirican, S.; Cilek, S.; Ciftçi, H.; Bıyıkoğlu, M.; Karaçınar, S.; Yokuş, A. Preliminary study on heavy metal concentrations of Anatolian Khramulya, *Capoeta tinca* (Heckel, 1843) from Çamlıgöze Dam Lake, Sivas, Turkey. *J. Environ. Health Sci. Eng.* **2013**, *11*, 7.

(18) Xu, Z.; Xu, X.; Tsang, D. C. W.; Cao, X. Contrasting impacts of pre- and post-application aging of biochar on the immobilization of Cd in contaminated soils. *Environ. Pollut.* **2018**, *242*, 1362−1370.

(19) Wang, Z.; Guo, H.; Shen, F.; Yang, G.; Zhang, Y.; Zeng, Y.; Wang, L.; Xiao, H.; Deng, S. Biochar produced from oak sawdust by Lanthanum (La)-involved pyrolysis for adsorption of ammonium (NH_4^+), nitrate (NO_3^-), and phosphate (PO_4^{3-}). *Chemosphere* **2015**, *119*, 646−653.

(20) Zhang, Y.; Pan, B.; Shan, C.; Gao, X. Enhanced phosphate removal by nanosized hydrated La(III) oxide confined in cross-linked polystyrene networks. *Environ. Sci. Technol.* **2016**, *50*, 1447−1454.

(21) Liu, X.; Zong, E.; Hu, W.; Song, P.; Wang, J.; Liu, Q.; Ma, Z.; Fu, S. Lignin-derived porous carbon loaded with $La(OH)_3$ nanorods for highly efficient removal of phosphate. *ACS Sustainable Chem. Eng.* **2019**, *7*, 758−768.

(22) Yang, Q.; Wang, X.; Luo, W.; Sun, J.; Xu, Q.; Chen, F.; Zhao, J.; Wang, S.; Yao, F.; Wang, D.; Li, X.; Zeng, G. Effectiveness and mechanisms of phosphate adsorption on iron-modified biochars derived from waste activated sludge. *Bioresour. Technol.* **2018**, *247*, 537−544.

(23) Xu, Q.; Chen, Z.; Wu, Z.; Xu, F.; Yang, D.; He, Q.; Li, G.; Chen, Y. Novel lanthanum doped biochars derived from lignocellulosic wastes for efficient phosphate removal and regeneration. *Bioresour. Technol.* **2019**, *289*, No. 121600.

(24) Wang, Z.; Shen, D.; Shen, F.; Li, T. Phosphate adsorption on lanthanum loaded biochar. *Chemosphere* **2016**, *150*, 1−7.

(25) Sun, X.; Guo, P.; Sun, Y.; Cui, Y. Adsorption of hexavalent chromium by sodium alginate fiber biochar loaded with lanthanum. *Materials* **2021**, *14*, 2224.

(26) Yin, H.; Wang, J.; Zhang, R.; Tang, W. Performance of physical and chemical methods in the co-reduction of internal phosphorus and nitrogen loading from the sediment of a black odorous river. *Sci. Total Environ.* **2019**, *663*, 68−77.

(27) Yin, T.; Zheng, Y.; Liu, T.; Wang, X.; Gao, J.; Nie, Z.; Song, L.; Xu, G.; Yuan, J. Study on water purification effect and operation parameters of various units of wastewater circulation. *Water* **2022**, *14*, 1743.

(28) Wu, B.; Fang, L.; Fortner, J. D.; Guan, X.; Lo, I. M. C. Highly efficient and selective phosphate removal from wastewater by magnetically recoverable $La(OH)_3/Fe_3O_4$ nanocomposites. *Water Res.* **2017**, *126*, 179−188.

(29) Hoslett, J.; Ghazal, H.; Katsou, E.; Jouhara, H. The removal of tetracycline from water using biochar produced from agricultural discarded material. *Sci. Total Environ.* **2021**, *751*, No. 141755.

(30) Zhang, Q.; Ying, G.; Pan, C.; Liu, Y.; Zhao, J. Comprehensive evaluation of antibiotics emission and fate in the river basins of China: source analysis, multimedia modeling, and linkage to bacterial resistance. *Environ. Sci. Technol.* **2015**, *49*, 6772−6782.

(31) Tran, N. H.; Chen, H.; Reinhard, M.; Mao, F.; Gin, K. Y. Occurrence and removal of multiple classes of antibiotics and antimicrobial agents in biological wastewater treatment processes. *Water Res.* **2016**, *104*, 461−472.

(32) Rilstone, V.; Vignale, L.; Craddock, J.; Cushing, A.; Filion, Y.; Champagne, P. The role of antibiotics and heavy metals on the development, promotion, and dissemination of antimicrobial resistance in drinking water biofilms. *Chemosphere* **2021**, *282*, No. 131048.

(33) Song, Z.; Zhuang, H.; Xiao, Z.; Suo, D. Residue accumulation, distribution, and withdrawal period of sulfamethazine and N-acetylsulfamethazine in poultry waste from broilers. *Chemosphere* **2021**, *278*, No. 130420.

(34) Zhang, G.; Wo, R.; Sun, Z.; Xiao, L.; Liu, G.; Hao, G.; Guo, H.; Jiang, W. Amido-functionalized magnetic metal-organic frameworks adsorbent for the removal of bisphenol A and tetracycline. *Front. Chem.* **2021**, *9*, No. 707559.

(35) Luo, Y.; Wang, Y.; Zhu, Y.; Xue, M.; Zheng, A.; Han, Y.; Yin, Z.; Hong, Z.; Xie, C.; Li, X.; Lei, S.; Gao, B. Ball-milled bismuth

https://doi.org/10.1021/acsomega.3c01251
ACS Omega 2023, 8, 29966−29978

oxychloride/biochar nanocomposites with rich oxygen vacancies for reactive red-120 adsorption in aqueous solution. *Biochar* **2022**, *4*, 21.
(36) Wu, Z.; Zhong, H.; Yuan, X.; Wang, H.; Wang, L.; Chen, X.; Zeng, G.; Wu, Y. Adsorptive removal of methylene blue by rhamnolipid-functionalized graphene oxide from wastewater. *Water Res.* **2014**, *67*, 330−344.
(37) Ngankam, E. S.; Dai-Yang, L.; Debina, B.; Baçaoui, A.; Yaacoubi, A.; Rahman, A. N. Preparation and characterization of magnetic banana peels biochar for fenton degradation of methylene blue. *Mater. Sci. Appl.* **2020**, *11*, 382−400.
(38) Akpotu, S. O.; Moodley, B. Synthesis and characterization of citric acid grafted MCM-41 and its adsorption of cationic dyes. *J. Environ. Chem. Eng.* **2016**, *4*, 4503−4513.
(39) Zhang, J.; Lü, F.; Shao, L.; He, P. The use of biochar-amended composting to improve the humification and degradation of sewage sludge. *Bioresour. Technol.* **2014**, *168*, 252−258.
(40) Wang, Y.; van Zwieten, L.; Wang, H.; Wang, L.; Li, R.; Qu, J.; Zhang, Y. Sorption of Pb(II) onto biochar is enhanced through co-sorption of dissolved organic matter. *Sci. Total Environ.* **2022**, *825*, No. 153686.
(41) Srocke, F.; Han, L.; Dutilleul, P.; Xiao, X.; Smith, D. L.; Mašek, O. Synchrotron X-ray microtomography and multifractal analysis for the characterization of pore structure and distribution in softwood pellet biochar. *Biochar* **2021**, *3*, 671−686.
(42) Sharef, H. Y.; Fakhre, N. A. Rapid adsorption of some heavy metals using extracted chitosan anchored with new aldehyde to form a schiff base. *PLoS One* **2022**, *17*, No. e0274123.
(43) Li, W.; Cheng, C.; He, L.; Liu, M.; Cao, G.; Yang, S.; Ren, N. Effects of feedstock and pyrolysis temperature of biochar on promoting hydrogen production of ethanol-type fermentation. *Sci. Total Environ.* **2021**, *790*, No. 148206.
(44) Pulka, J.; Manczarski, P.; Stępień, P.; Styczyńska, M.; Koziel, J. A.; Białowiec, A. Waste-to-carbon: is the torrefied sewage sludge with high ash content a better fuel or fertilizer? *Materials* **2020**, *13*, 954.
(45) Zhang, L.; Ren, Y.; Xue, Y.; Cui, Z.; Wei, Q.; Han, C.; He, J. Preparation of biochar by mango peel and its adsorption characteristics of Cd(ii) in solution. *RSC Adv.* **2020**, *10*, 35878−35888.
(46) Li, X.; Jiang, Y.; Chen, T.; Zhao, P.; Niu, S.; Yuan, M.; Ma, X. Adsorption of norfloxacin from wastewater by biochar with different substrates. *Environ. Geochem. Health* **2022**, DOI: 10.1007/s10653-022-01414-6.
(47) Liu, W.; Ren, D.; Wu, J.; Wang, Z.; Zhang, S.; Zhang, X.; Gong, X. Adsorption behavior of 2,4-DCP by rice straw biochar modified with CTAB. *Environ. Technol.* **2021**, *42*, 3797−3806.
(48) Wang, J.; Dou, M.; Wang, X.; Gao, B.; Zhuang, T.; Ma, Z. Synergetic mechanism of defective g-C_3N_4 activated persulfate on removal of antibiotics and resistant bacteria: ROSs transformation, electron transfer and noncovalent interaction. *Chemosphere* **2022**, *294*, No. 133741.
(49) Zhao, C.; Ma, J.; Li, Z.; Xia, H.; Liu, H.; Yang, Y. Highly enhanced adsorption performance of tetracycline antibiotics on KOH-activated biochar derived from reed plants. *RSC Adv.* **2020**, *10*, 5066−5076.
(50) Li, Z.; Wang, Z.; Wu, X.; Li, M.; Liu, X. Competitive adsorption of tylosin, sulfamethoxazole and Cu(II) on nano-hydroxyapatitemodified biochar in water. *Chemosphere* **2020**, *240*, No. 124884.
(51) Song, J.; Messele, S. A.; Meng, L.; Huang, Z.; Gamal El-Din, M. Adsorption of metals from oil sands process water (OSPW) under natural pH by sludge-based Biochar/Chitosan composite. *Water Res.* **2021**, *194*, No. 116930.
(52) Xu, Z.; Xiang, Y.; Zhou, H.; Yang, J.; He, Y.; Zhu, Z.; Zhou, Y. Manganese ferrite modified biochar from vinasse for enhanced adsorption of levofloxacin: Effects and mechanisms. *Environ. Pollut.* **2021**, *272*, No. 115968.
(53) Liu, L.; Li, X.; Wang, X.; Wang, Y.; Shao, Z.; Liu, X.; Shan, D.; Liu, Z.; Dai, Y. Metolachlor adsorption using walnut shell biochar modified by soil minerals. *Environ. Pollut.* **2022**, *308*, No. 119610.
(54) Zhao, M.; Dai, Y.; Zhang, M.; Feng, C.; Qin, B.; Zhang, W.; Zhao, N.; Li, Y.; Ni, Z.; Xu, Z.; Tsang, D. C. W.; Qiu, R. Mechanisms of Pb and/or Zn adsorption by different biochars: Biochar characteristics, stability, and binding energies. *Sci. Total Environ.* **2020**, *717*, No. 136894.
(55) Rajapaksha, A. U.; Vithanage, M.; Ahmad, M.; Seo, D. C.; Cho, J. S.; Lee, S. E.; Lee, S. S.; Ok, Y. S. Enhanced sulfamethazine removal by steam-activated invasive plant-derived biochar. *J. Hazard. Mater.* **2015**, *290*, 43−50.
(56) Wang, Y.; Zheng, Y.; Qian, X.; Yang, X.; Chen, J.; Wu, W. Influence of volcanic stone and Al@TCAP-N on the purification effect of primary precipitation units. *J. Agro-Environ. Sci.* **2020**, *39*, 2868−2877.
(57) Zheng, Y.; Wang, Y.; Yang, X.; Gao, J.; Xu, G.; Yuan, J. Effective mechanism of water purification effect of nitrogen-modified attapulgite, volcanic stone and the combined exogenous micro-organisms. *Front. Microbiol.* **2022**, *13*, No. 944366.
(58) Ambaye, T. G.; Vaccari, M.; van Hullebusch, E. D.; Amrane, A.; Rtimi, S. Mechanisms and adsorption capacities of biochar for the removal of organic and inorganic pollutants from industrial wastewater. *Int. J. Environ. Sci. Technol.* **2021**, *18*, 3273−3294.
(59) Jiang, T.; Wang, B.; Gao, B.; Cheng, N.; Feng, Q.; Chen, M.; Wang, S. Degradation of organic pollutants from water by biochar-assisted advanced oxidation processes: Mechanisms and applications. *J. Hazard. Mater.* **2023**, *442*, No. 130075.
(60) Hoslett, J.; Ghazal, H.; Mohamad, N.; Jouhara, H. Removal of methylene blue from aqueous solutions by biochar prepared from the pyrolysis of mixed municipal discarded material. *Sci. Total Environ.* **2020**, *714*, No. 136832.
(61) Zhang, P.; O'Connor, D.; Wang, Y.; Jiang, L.; Xia, T.; Wang, L.; Tsang, D. C. W.; Ok, Y. S.; Hou, D. A green biochar/iron oxide composite for methylene blue removal. *J. Hazard. Mater.* **2020**, *384*, No. 121286.
(62) Xi, J.; Zhang, R.; Ye, L.; Du, X.; Lu, X. Multi-step preparation of Fe and Si modified biochar derived from waterworks sludge towards methylene blue adsorption. *J. Environ. Manage.* **2022**, *304*, No. 114297.
(63) Diaz-Uribe, C.; Walteros, L.; Duran, F.; Vallejo, W.; Romero Bohórquez, A. R. *Prosopis juliflora* seed waste as biochar for the removal of blue methylene: a thermodynamic and kinetic study. *ACS Omega* **2022**, *7*, 42916−42925.
(64) Deng, J.; Dong, H.; Zhang, C.; Jiang, Z.; Cheng, Y.; Hou, K.; Zhang, L.; Fan, C. Nanoscale zero-valent iron/biochar composite as an activator for Fenton-like removal of sulfamethazine. *Sep. Purif. Technol.* **2018**, *202*, 130−137.
(65) Tian, W.; Lin, J.; Zhang, H.; Duan, X.; Wang, H.; Sun, H.; Wang, S. Kinetics and mechanism of synergistic adsorption and persulfate activation by N-doped porous carbon for antibiotics removals in single and binary solutions. *J. Hazard. Mater.* **2022**, *423*, No. 127083.
(66) Lin, L.; Jiang, W.; Xu, P. Comparative study on pharmaceuticals adsorption in reclaimed water desalination concentrate using biochar: Impact of salts and organic matter. *Sci. Total Environ.* **2017**, *601-602*, 857−864.

https://doi.org/10.1021/acsomega.3c01251
ACS Omega 2023, 8, 29966−29978